Boundary Layer Separation Effects on Viscous Oblique Detonations over Compression Corners

Xinke Shao, Zijian Zhang*, Jiaao Hao, Chih-yung Wen
Department of Aeronautical and Aviation Engineering, The Hong Kong Polytechnic University,
Hong Kong, China.

1 Introduction

In the majority of the previous studies pertinent to oblique detonation waves (ODWs), the viscosity and incoming boundary layer effects are absent. Recently, it was found that viscosity effects are non-negligible when there are flow separations [1-3]. When boundary layer separation occurs, the separation bubble will introduce additional upstream disturbance to ODWs. This may change the initiation structure of the ODWs. In this current work, the viscosity and incoming boundary layer are considered to evaluate their effects on ODW initiation structures.

2 Method

The reactive Navier-Stokes equations are solved with the compressible solver PHAROS [4], an in-house massively parallel block-structured finite-volume code solving the conservation equations of mass, momentum, energy and species transport. The Wilcox k–ω turbulence model is used to describe the turbulent flow. The freestream static pressure and temperature are fixed as p_∞=1 bar and T_∞=800 K. The equivalence ratio is fixed as ER=0.3. Supersonic freestream conditions of Ma 3.4 and Ma 3.8 are considered, under which an abrupt and smooth ODW can be formed respectively with incoming boundary layer absent. The two-dimensional computational domain is shown in Figure.1. It is comprised of a fore flat plate with different lengths (L_p) and a rear ramp with 25°deflection angle. Freestream conditions are adopted on the far field. Non-slip non-catalytic isothermal wall condition is adopted for the solid surfaces, where the wall to recovery temperature ratio is fixed as T_w/T_R=0.35. Zero-gradient boundary condition is enforced at the outflow.

Correspondence to: zjzhanglw@gmail.com (Z.Zhang)

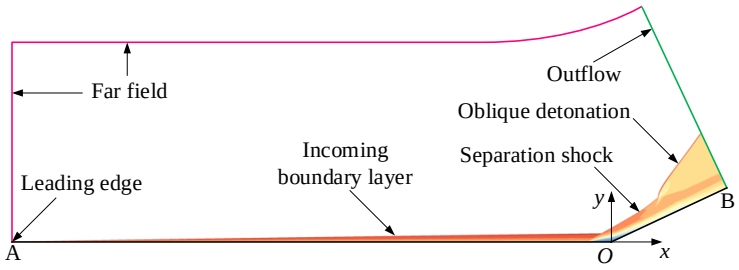

Figure. 1: Schematic diagram of the computation domain and boundary conditions

3 Structures of separation-free ODWs

To validate the solver, the hypervelocity projectile-induced ODW experiment conducted by Verreault and Higgins [5] is first numerically replicated. In the experiment, a projectile with a diameter of 12.7 mm, a half-cone angle of 40°, and a velocity of 2180 m/s was launched into a quiescent explosive gas mixture ($2H_2 + O_2 + 7Ar$) at 298 K and 101 kPa. The numerical and the experimental results are compared in Figure.2. As seen, the ODW structure is well captured numerically.

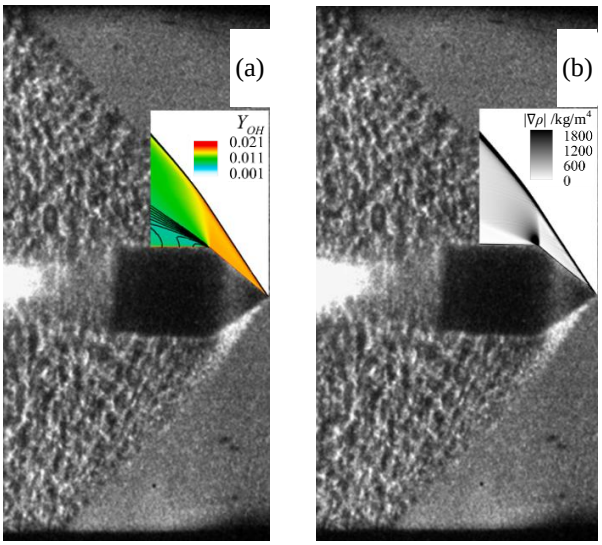

Figure. 2 Comparison of experimental [5] and numerical results: (a) contour of OH mass fraction overlaid with pressure isolines (b) density gradient magnitude.

Steady state solutions are then examined for the L_p=0 m reactive cases, where the fore plate has zero length, and hence, no corner-induced separation can be formed. These cases involve only combustion features but no separation and serve as referential cases. Two Mach number conditions (*Ma* 3.4 & *Ma* 3.8) are considered to cover both abrupt and smooth ODWs. The flow field in terms of pressure (p/p_∞), temperature (T/T_∞) and hydrogen mass fraction (Y_{H2}) are shown in Figure.3. It is observed that an abrupt ODW is formed at a relative low Mach number of *Ma* 3.4 (U_∞/D_{CJ}=1.44), while a smooth one is formed at higher Mach number of *Ma* 3.8 (U_∞/D_{CJ}=1.61).

Generally, the main difference between an abrupt and a smooth ODW lies in the presence of the primary transverse wave (PTW). The wave angle difference between OSW and ODW is larger in the *Ma* 3.4 case, hence a PTW is generated therein to match the great pressure difference between the post-OSW and -ODW states. The PTW in the abrupt ODW will reflect on the wall, forming a reflected shock and generating additional pressure rise and adverse pressure gradient on the wall. This is further

demonstrated in Figure.4, where the pressure (p/p_∞) and progress variable (C) near the wall are plotted for both the *Ma* 3.4 and *Ma* 3.8 case. The progress variable C is obtained based on species mass fraction, where C=0 indicates no reaction, whereas C=1 means complete reaction. For both cases, the pressure profile first undergoes a drastic jump given by the inert, ramp-induced OSW, followed by a plateau. The plateau has almost constant pressure that agrees well with the analytical solutions from oblique shock relations. This plateau region is referred to as an induction zone in previous studies since there are not sufficient combustion intermediates to trigger autoignition. After the plateau, a relative moderate pressure rise is formed synchronically with the autoignition phenomenon indicated by a sudden increase in C. For both cases, the pressure rise after the OSW starts at C=0.01 and peaks at C=0.99. This evidences that the moderate pressure rise following the plateau is caused by rapid heat release of deflagration waves. Moreover, pressure drops slightly after C=0.99 because the heat release is no longer intense enough to counteract thermal expansion [6]. What makes the abrupt ODW different from the smooth one is an extra sudden pressure rise at about s=0.017 m. This spike is attributed to the PTW impinging towards the wall.

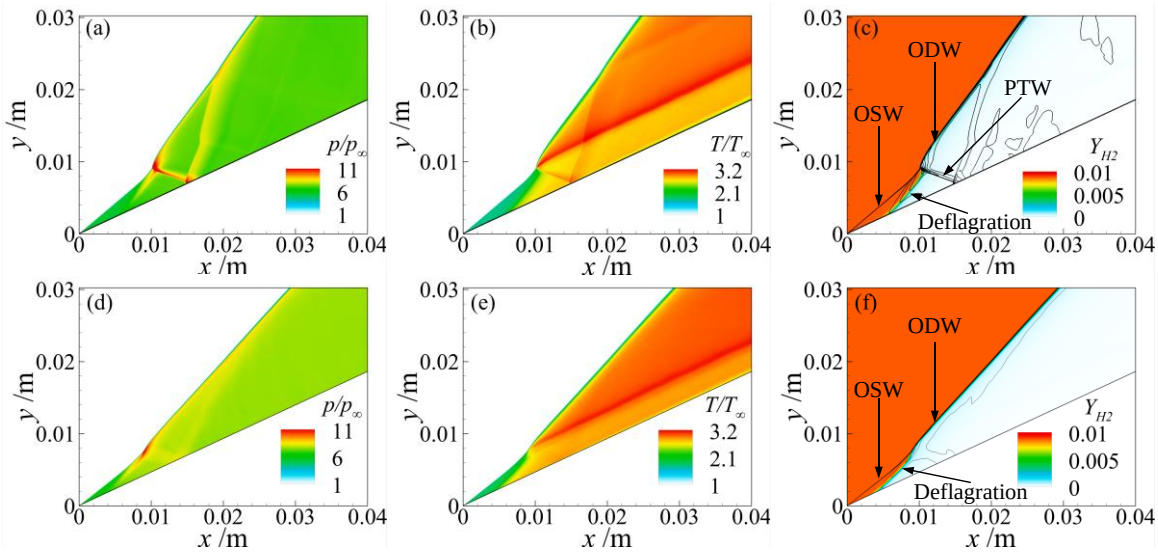

Figure. 3 Steady-state flow field of the oblique detonation structures in L_p=0 m cases. (a)-(c): *Ma* 3.4, (d)-(f): *Ma* 3.8.

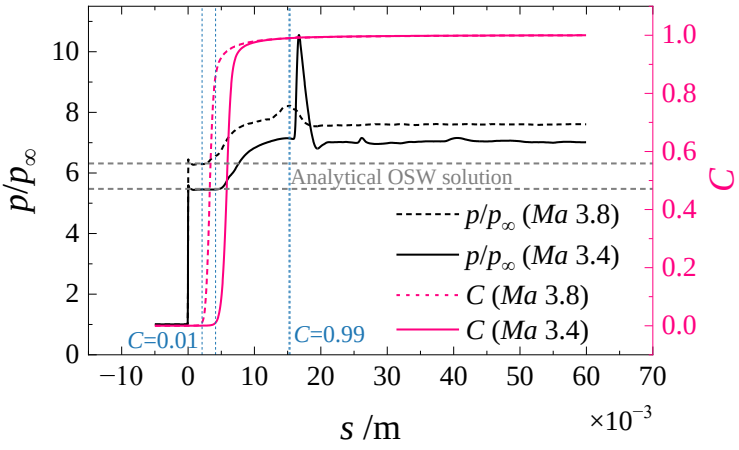

Figure. 4 Pressure and progress variable distribution near the wall.

4 Flow structures of ODWs with separations

The cases with a fore flat plate length of L_p=0.3 m is examined next to qualitatively assess the effects of incoming boundary layer on combustion structures. The steady-state flow in terms of temperature (T/T_∞), hydrogen mass fraction (Y_{H2}) and streamwise velocity (u/u_∞) are plotted in Figure.5. Generally, an abrupt and a smooth ODW are still successfully initiated and stabilized in the *Ma* 3.4 and *Ma* 3.8 cases. A separation bubble is formed at the compression corner because sufficient adverse pressure gradient is imposed onto the incoming boundary layer by the ramp-induced inert oblique shock. The deflagration surfaces also move upstream to the front of the separation bubble.

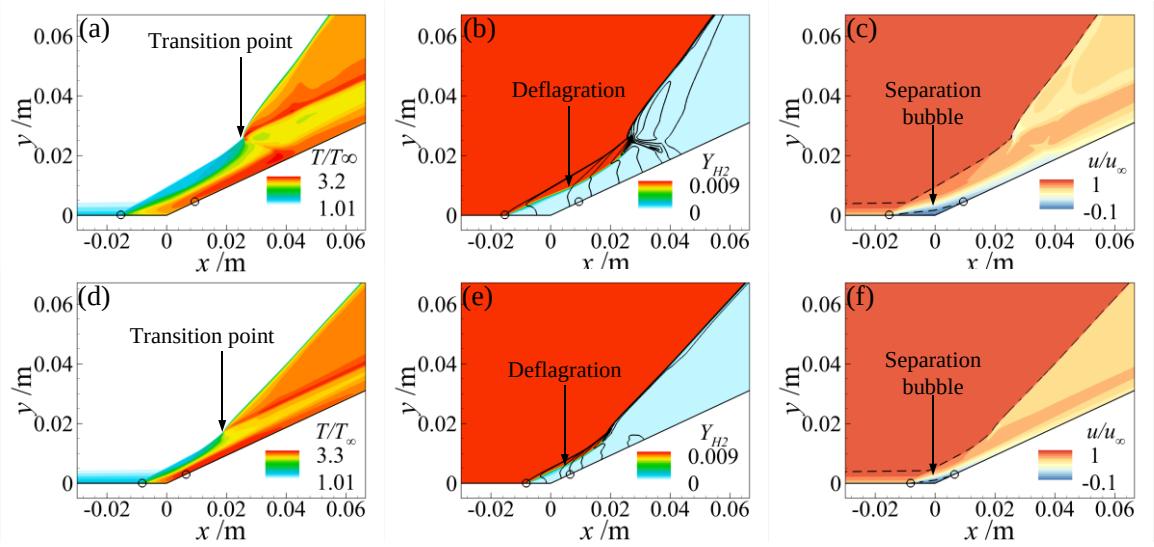

Figure. 5 Steady states of the flow field in the L_p=0.3 m cases. (a)-(c): *Ma* 3.4, (d)-(f): *Ma* 3.8. The separation and reattachment points are marked with open circles. Solid isolines in (b) and (e) are pressure isolines. Dashed lines in (c) and (f) represent isolines of u/u_∞=0.99 and u/u_∞=0.

Figure.6 further plots the numerical schlieren of the above two reactive cases (L_p=0 m and L_p=0.3 m) to show the wave and flame structures at *Ma* 3.4 and *Ma* 3.8. An additional inert case (L_p=0.3 m) is also plotted for reference. Despite the presence of PTW, the flow and combustion structures in the *Ma* 3.4 and *Ma* 3.8 cases are generally similar. Therefore, the following discussion will be based on the *Ma* 3.4 series.

The effects of separation on combustion can be demonstrated by comparing the first two columns in Figure.6. As seen, when flow separation occurs, the autoignition locus on the wall moves upstream from about x=0.005 m in the L_p=0 m case to x=-0.017 m in the L_p=0.3 m case. This is because the ignition delay time is shortened in thermal boundary layer whilst velocity is diminished within the velocity boundary layer. As a result, the autoignition length is reduced within the boundary layer, leading to the advancement of the deflagration surfaces. Moreover, the OSW-ODW transition point moves downstream from about X_t=0.01 m in the L_p=0 m case to X_t=0.025 m in the L_p=0.3 m case. This is because the separation bubble plays a role as an aerodynamic wedge with smaller deflection angle. With smaller deflection angle comes lower pressure and temperature rise ratio across the OSW. Therefore, the ignition delay within the induction region is lowered, the OSW-ODW transition point recedes. Comparing the second and third column in Figure.6, it can also be easily found the occurrence of combustion also has a significant impact on the separation structures. Upon the occurrence of ignition, the separation length is increased from around 0.002 m to 0.016 m in the *Ma* 3.4 case. This separation amplification phenomenon can be attributed to the additional adverse pressure gradient given by deflagration as discussed in Figure.4.

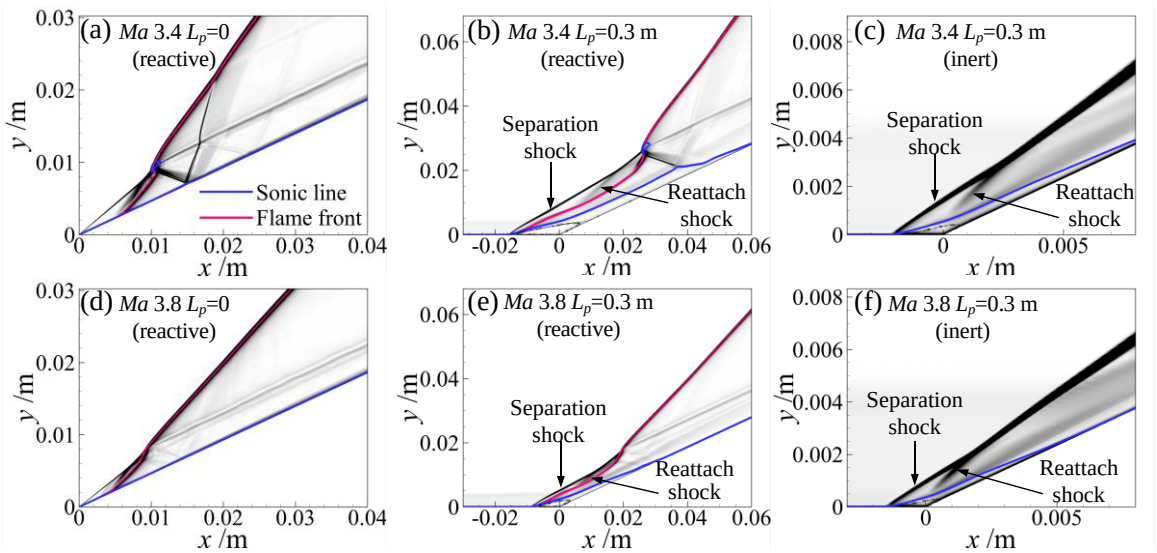

Figure. 6 Numerical schlieren ($|\nabla\rho|$) of the reactive and inert cases at (a)-(c) *Ma* 3.4 and (d)-(f) *Ma* 3.8.

The wall properties of the *Ma* 3.4 and *Ma* 3.8 reactive cases and their inert counterpart are presented in Figure.7 to further assess the effects of combustion on separation. C_f, C_p and St denote skin friction coefficient, wall pressure coefficient and Stanton number respectively. $St=\frac{q_w}{0.5\rho_\infty u_\infty^3}$, where q_w is the wall heat flux. For both the abrupt and smooth ODW, the results are qualitatively similar. When combustion occurs the separation bubble grows larger and wall pressure and Stanton number is markedly increased. The growth of separation bubble is due to additional adverse pressure gradient imposed by deflagration energy release. This is analogous to what is discussed in Figure.4 and is further evidenced in Figure.7 (b) and (e). The pressure rise at the separation points remains fixed whilst the plateau pressure is significantly enhanced when combustion occurs. Moreover, in the reactive case, deflagration surfaces are present ahead of the separation bubble. As such, the separation bubble temperature is elevated, leading to higher wall heat flux and Stanton number.

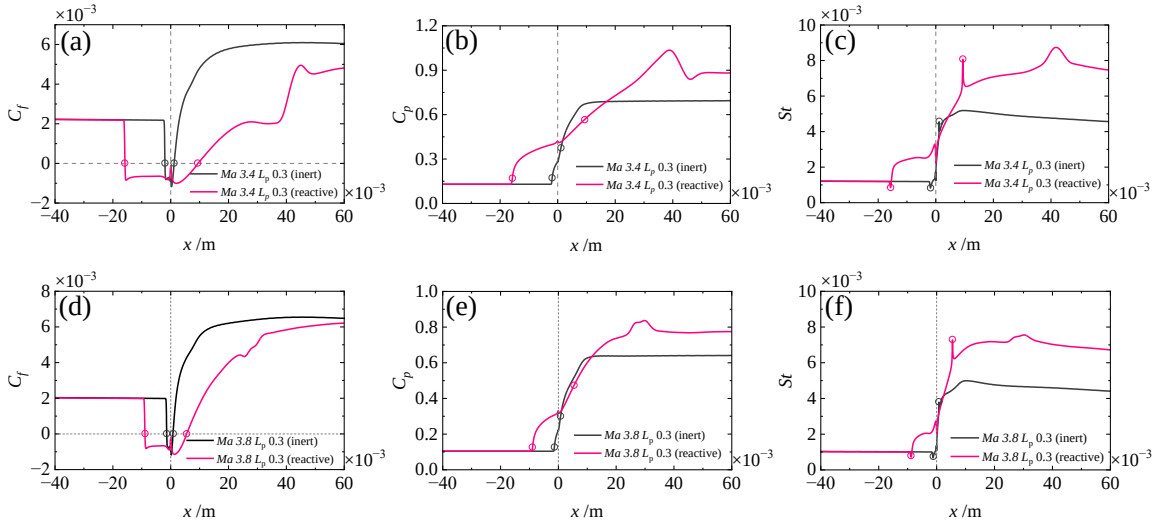

Figure. 7 Skin friction coefficient (C_f), wall pressure coefficient (C_p) and Stanton number (St) of (a)-(c): *Ma* 3.4 series and (d)-(f): *Ma* 3.8 series. Open circles indicate the separation and reattachment points.

5 Conclusions

Supersonic viscous reactive flows over compression corners can be characterized by two features. One is boundary layer separation due to adequate adverse pressure gradient given by flow deflection and oblique shock formation at the corner. The other is the combustion phenomenon behind the shock, that is, the auto-ignition of deflagration due to shock compression and the onset of detonation due to deflagration acceleration. In this study, it is found that the shock-induced separation and combustion are coupled. When separation occurs, the deflagration surface moves upstream due to shorter ignition delay within the boundary layer. The deflagration surface is eventually stabilized ahead of the separation bubble. Rapid energy release by deflagration elevates the wall plateau pressure and imposes additional adverse pressure gradient. As a result, the separation bubble grows larger. The presence of separation bubbles reduces the temperature and increases the ignition delay in the induction zone. This further leads to the recession of OSW-ODW transition point.

Acknowledgments

This work is supported by the National Natural Science Foundation of China (Grant no. 12202374 and no. 12472239) and the Hong Kong Research Grants Council (no. 15204322).

References

[1] Fang, Yishen, Zijian Zhang, and Zongmin Hu. "Effects of boundary layer on wedge-induced oblique detonation structures in hydrogen-air mixtures." International Journal of Hydrogen Energy 44.41 (2019): 23429-23435.

[2] Bachman, Christian L., and Gabriel B. Goodwin. "Ignition criteria and the effect of boundary layers on wedge-stabilized oblique detonation waves." Combustion and Flame 223 (2021): 271-283.

[3] Miao, Shikun, et al. "Shock wave-boundary layer interactions in wedge-induced oblique detonations." Combustion Science and Technology 192.12 (2020): 2345-2370.

[4] Hao, Jiaao, Jingying Wang, and Chunhian Lee. "Numerical study of hypersonic flows over reentry configurations with different chemical nonequilibrium models." *Acta Astronautica* 126 (2016): 1-10.

[5] Verreault, Jimmy, and Higgins, Andrew J. "Initiation of detonation by conical projectiles." Proceedings of the Combustion Institute 33.2 (2011): 2311-2318.

[6] Li, Chiping, K. Kailasanath, and Elaine S. Oran. "Detonation structures behind oblique shocks." Physics of Fluids 6.4 (1994): 1600-1611.